

18 **ABSTRACT**

19 Macrophages, a class of tissue resident innate immune cells, are responsible for sequestering
20 foreign objects through the process of phagocytosis, making them a promising target for immune-
21 modulation via particulate engineering. Here, we report that nanoparticle (NP) dosing and cellular
22 internalization via phagocytosis significantly enhances survival of *ex vivo* cultures of primary bone
23 marrow-derived, alveolar, and peritoneal macrophages over particle-free controls. The enhanced
24 survival is attributed to suppression of caspase-dependent apoptosis and is linked to phagocytosis
25 and lysosomal signaling, which was also found to occur *in vivo*. Uniquely, poly(ethylene glycol)-
26 based NP treatment does not alter macrophage polarization or lead to inflammatory effects. The
27 enhanced survival phenomenon is also applicable to NPs of alternative chemistries, indicating the
28 potential universality of this phenomenon with relevant drug delivery particles. These findings
29 provide a framework for extending the lifespan of primary macrophages *ex vivo* for drug screening,
30 vaccine studies, and cell therapies and has implications for any *in vivo* particulate immune-
31 engineering applications.

32

33 **KEYWORDS**

34 Macrophage, Survival, Apoptosis, Nanoparticles, Longevity, Phagocytosis

35 INTRODUCTION

36 Macrophages are leukocytes responsible for phagocytosing foreign objects, bacteria, and apoptotic
37 cells, maintaining homeostasis, and bridging innate and adaptive immunities[1]. Hence,
38 macrophages represent significant therapeutic targets and control of their phenotype, activity, and
39 persistence could promote treatment for a wide range of conditions. Macrophages are highly
40 responsive to their microenvironment and are equipped with phagocytic capabilities that enable
41 them to internalize pathogens and larger particulates. Phagocytosis begins with ligand binding to
42 cell surface receptors, triggering cytoskeletal rearrangement and actin polymerization to surround
43 the target object. The target is then internalized within a phagosome, initiating a degradation
44 process that proceeds through acidification of the compartment and lysosomal fusion[2]. Thus, the
45 cell receives a plethora of information during phagocytosis that is critical to regulating cell
46 function; however, decoupling the highly interconnected signaling pathways to precisely tune cell
47 response remains an ongoing challenge.

48
49 Nano- and microparticles are natural avenues to stimulate macrophage function and elicit
50 therapeutic response by leveraging these inherent phagocytic capabilities and delivering precision
51 cues initiated during phagocytosis[3, 4]. Macrophages are highly sensitive to the cell-material
52 interface, where everything from surface charge to particle shape can influence subsequent
53 downstream signaling[5, 6]. Unsurprisingly, the role of material selection is critically important to
54 tuning and directing these responses. Some materials used to fabricate nano- and microparticles
55 have been shown to cause strong inflammatory or toxic effects on macrophages[7], while recent
56 advances in biomaterials have elucidated classes of modular materials with strong
57 biocompatibility[8-11]. Early generations of particulate therapeutics sought engineering solutions
58 that avoided internalization by phagocytic immune cells to ensure successful cargo delivery[12,
59 13]; however, an emerging alternative is to promote controlled interactions with innate immune
60 cells to regulate immune response[14, 15]. Indeed, particulates with no added stimulatory or
61 tolerizing moieties show anti-inflammatory effects for preclinical treatment for West Nile virus,
62 inflammatory bowel disease[16], sepsis[17], and acute lung injury[13, 18] that is presumably
63 driven by particle phagocytosis and subsequent cell “distraction” of inflammatory phagocytes of
64 monocytes and neutrophils, respectively.

65

66 Given the highly interconnected role between phagocytosis and macrophage phenotype, we sought
67 to study downstream effects of primary macrophage internalization with “immunologically inert”
68 poly(ethylene glycol) (PEG) diacrylate (PEGDA)-based nanoparticles (NPs), to uniquely
69 investigate NP internalization in the absence of any known stimulatory cue, such as toll-like
70 receptor (TLR) agonists or autophagy signals. Here, we report a surprising link between cell
71 viability and particle phagocytosis in the absence of cell activation, allowing us to dramatically
72 extend the viability of *ex vivo* macrophage cultures through particle treatment. We show that a
73 single dose of NPs significantly delays primary macrophage cell death through the downregulation
74 of caspase-dependent apoptotic pathways and activation of MAPK cascades, with no major
75 changes to macrophage activation phenotype following NP uptake. Similar mechanisms are
76 observed following *in vivo* administration, with the enhanced survival phenomenon occurring in
77 *ex vivo* cultures of terminally differentiated macrophages isolated from tissue, as well as particles
78 of alternative chemistries, indicating the potential universality of this phenomenon to any subset
79 of macrophages with relevant drug delivery particles. Overall, this work uniquely demonstrates
80 the ability of NPs to suppress apoptotic signaling and prolong viability in primary macrophages
81 through phagocytosis signaling. This work could eliminate a major obstacle for macrophage-based
82 cell immunotherapies and drug screenings that are typically hindered by poor macrophage
83 survival, as well as provide mechanistic insight into the implications of NP phagocytosis on cell
84 longevity for a wide range of therapeutic applications.

85

86 **RESULTS**

87 **PEGDA NP phagocytosis stimulates primary macrophage survival *ex vivo*.** As shown in
88 **Figure 1A**, we observed that bone marrow-derived macrophages (BMMs) can persist in culture
89 for up to 115 days following treatment with a single 20 $\mu\text{g/ml}$ dose inert, unfunctionalized PEGDA
90 NPs. This contrasts with untreated BMMs, which do not survive beyond a few weeks in culture.
91 PEGDA NPs, approximately 300 nm in hydrodynamic size, were characterized using dynamic
92 light scattering (DLS), scanning electron microscopy (SEM), and assayed for endotoxin levels that
93 were determined to be non-significant (**Figure S1, S2**). To determine whether BMM survival is
94 dependent on NP concentration, BMMs were incubated with a single dose of PEGDA NPs at
95 concentrations ranging between zero and 100 $\mu\text{g/ml}$ and survival was determined through
96 metabolic activity as a measure of cell viability. From cell viability results, BMM survival was

97 determined to be a strong function of NP concentration. One week following NP treatment, 20
98 $\mu\text{g/ml}$ PEGDA NPs showed a 1.5x higher cell viability relative to untreated BMMs ($p\text{-value}<0.05$)
99 while 50 and 100 $\mu\text{g/ml}$ NP concentrations caused 3x and 3.5x higher cell viability compared to
100 untreated BMMs ($p\text{-value}<0.0001$), respectively (**Figure 1B**). At a two-week timepoint, BMMs
101 treated with 100 $\mu\text{g/ml}$ and 50 $\mu\text{g/ml}$ of NPs showed $\sim 2.8\text{x}$ and 2.2x higher cell viability relative
102 to untreated BMMs, respectively ($p\text{-value}<0.0001$), while the cell viability of BMMs treated with
103 NPs at concentrations less than 50 $\mu\text{g/ml}$ was statistically indistinguishable from cell viability of
104 untreated BMMs. BMM count data were in agreement with cell viability as measured by metabolic
105 activity and reflected strong NP concentration-dependent maintenance of BMM counts (**Figure**
106 **1C**). Furthermore, NPs treated to BMMs in the absence of fetal bovine serum showed no statistical
107 differences in the resultant enhanced viability compared to BMMs in the presence of serum
108 (**Figure S3**).

109
110 To investigate whether the PEGDA NP-driven enhanced survival is applicable to NPs of varying
111 compositions, BMMs were dosed with 100 $\mu\text{g/ml}$ silver, gold, silica, and polystyrene NPs and cell
112 counts were used to evaluate survival after one week. All the tested NPs resulted in statistically
113 significantly higher cell counts than untreated BMMs (**Figure 1D**). BMMs treated with
114 polystyrene NPs had the highest counts and more than 10x the counts of untreated BMMs with $p\text{-value}<0.0001$
115 using Dunnett's multiple comparisons test as part of a one-way ANOVA. Silica and
116 silver NPs resulted in approximately 6x higher cell counts compared to untreated BMMs with $p\text{-value}<0.0001$.
117 BMMs treated with gold NPs had approximately 4x higher numbers than untreated
118 cells with $p\text{-value}<0.001$ while PEGDA NPs showed the smallest improvement yet statistically
119 significant with $p\text{-value}<0.01$ and around 3x higher counts of PEGDA NP-treated BMMs
120 compared to untreated cells. All NP stocks were evaluated for the presence of endotoxin (**Figure**
121 **S2**), with only silver and polystyrene detectable over the baseline. Overall, these results show that
122 enhanced survival is possible with many NP formulations and are not restricted to PEGDA or
123 polymeric NPs.

124
125 NP-viability enhancement to *ex vivo* survival was not restricted to BMMs. Murine alveolar
126 macrophages treated with a single dose of 100 $\mu\text{g/ml}$ NPs on day 1 show significantly higher
127 counts than untreated cells ($p\text{-value}<0.01$) three weeks following isolation from murine lungs

128 **(Figure 1E)**. Similarly, peritoneal macrophages treated with 100 µg/ml of NPs display *ex vivo*
129 longevity three weeks following isolation and a single dosage on day 1 (p-value<0.05) **(Figure**
130 **1F)**. Results from NP-driven longevity of alveolar and peritoneal macrophages combined with
131 those of BMMs highlight the versatility of utilizing NPs for enhancing the *ex vivo* survival of any
132 macrophage type.

133
134 **NP-dependent survival is not dependent on macrophage polarization.** Flow cytometric
135 analysis of M1 and M2 markers was executed on BMMs of different initial polarization states 24
136 hours following NP treatment (Representative gating of flow cytometric data in **Figure S4**). No
137 significant changes were observed in expression of either representative M1 markers (CD38,
138 CD86) or M2 markers (CD206, EGR2) in NP-treated BMMs **(Figures S5A-D)** according to a
139 student's T-test (p-value>0.05) indicating no considerable M1 or M2 polarization of BMMs
140 because of NP phagocytosis. Further, pre-skewed M1 and M2 BMMs treated with NPs did not
141 display any significant change in CD38, CD86, CD206, and EGR2 expression, indicating that
142 PEGDA NP phagocytosis promotes the survival of macrophages *ex vivo* without affecting their
143 polarization state. Increased expression of MHCII was observed in M0, M1, and M2 BMMs
144 **(Figure 2A)**, indicating the potential enhancing of antigen presentation in NP-treated macrophages
145 of all the tested phenotypes.

146
147 RNA sequencing (RNAseq) analysis was performed to identify relevant differentially expressed
148 genes (DEGs) and perform functional classifications and clustering to determine significant cell
149 processes involved in cell-NP interactions that ultimately lead to enhanced survival. Gene
150 expression in BMMs treated with 100 µg/ml NPs for 24 hours was compared to that of untreated
151 BMMs under the same culture conditions. Of the DEGs analyzed, 331 were determined to be
152 statistically significant with q-value<0.05, but fold change values were relatively low, ranging
153 between -2 and 2. The database for annotation, visualization and integrated discovery (DAVID),
154 was used to identify enriched gene ontology (GO) terms in the 331 significant DEGs. Full DAVID
155 enrichment analysis of GO terms is represented in **Table S1** (Selected significant GO terms in
156 **Figure S6**). DEGs in the Immune System Process GO term were used to guide our subsequent
157 analysis. RNAseq analysis confirms MHCII upregulation (*H2-ABI* gene) and points to a small
158 panel of 15 genes involved in immunity and regulating immune cell function **(Figure 2B)**.

159 However, potent changes to characteristic inflammatory genes were notably absent from this
160 panel, which confirms conclusions from flow cytometric analyses of polarization markers showing
161 little effect of NP treatment on macrophage activation phenotype. Further multiplex analysis of
162 M0 macrophage supernatants for a broad array of cytokines and chemokines only identified
163 detectable levels of IP-10, KC, MCP-1, MIP-2, VEGF, TNF- α in supernatants of untreated or NP-
164 treated BMMs (**Figure S5E**). However, no significant change in any cytokine levels in BMMs
165 treated with 100 μ g/ml PEGDA NPs was observed compared to their untreated counterparts as
166 determined by student's T-tests ($p>0.05$). These results support conclusions from flow cytometric
167 analyses indicating no notable impact of PEGDA NP phagocytosis on macrophage activation
168 phenotype and that the NP-induced macrophage longevity does not require macrophage activation
169 and/or classical polarization pathways.

170
171 While macrophage polarization was not required to observe the enhanced viability, long-living
172 NP-treated cells were observed to respond appropriately to immune stimuli. As shown **Figure 2C**
173 we observed that long living macrophages treated with 100 μ g/ml PEGDA NPs were able to
174 provide response to LPS challenge four weeks following NP treatment. Treated cells produced
175 expected cytokines of IL-6 and TNF- α (**Figure 2C**) in culture supernatants that are statistically
176 significant compared to untreated cells (as determined by student's T-tests p -values <0.01 and 0.05 ,
177 respectively).

178
179 **PEGDA NP treatment suppresses apoptotic pathways and promotes pro-survival signaling**
180 **in *ex vivo* macrophages.** In accordance with literature, untreated BMMs were found to undergo
181 apoptosis[19], or programmed cell death, that was delayed following NP treatment. Quadrant
182 analysis after 24 hours in culture revealed rapid cell death through apoptosis of untreated cells
183 (**Figure 3A, S7**). Treatment with 100 μ g/ml NPs showed retardation of all major quantified modes
184 of cell death, which was corroborated by suppression of active pro-apoptotic caspase 3/7
185 expression, an indicator of early apoptosis, in BMMs treated with NPs in a concentration-
186 dependent manner (**Figure 3B**). Three days following treatment with 100 μ g/ml NPs resulted in a
187 significantly lower active caspase 3/7 expression (p -value <0.01), while the margin of active
188 caspase 3/7 reduction is diminished with lower NP concentrations. TUNEL analysis revealed DNA
189 damage only in untreated cells, which occurs during the late stages of apoptosis. At 24 hours NP-

190 treated BMMs showed considerably lower fluorescent TUNEL signal than untreated BMMs
191 (**Figure 3C**), indicating lower late apoptosis characterized by DNA damage in BMMs treated with
192 NPs, which is also supported by analysis at 72 hours (**Figure S8**).

193
194 RNAseq results were further evaluated to provide insight into the factors contributing to apoptosis
195 suppression. Analysis of RNAseq revealed upregulation of several anti-apoptotic genes in NP-
196 treated BMMs including *BCL2-L1* (**Figure 3D**) indicating a cascade of anti-apoptotic signaling is
197 involved in promoting survival of *ex vivo* cultures of macrophages following NP treatment. In
198 addition, several pro-apoptotic genes were downregulated in NP-treated BMMs, most notably Bcl-
199 2-modifying factor (*BMF*) gene, which provides additional evidence to support the ability of NPs
200 to suppress apoptotic signaling in macrophages *ex vivo*. Furthermore, flow cytometric analysis on
201 BMMs treated with 100 µg/ml NPs for 3 days revealed significant upregulation of expression of
202 B cell lymphoma-2 (Bcl-2) anti-apoptotic protein relative to untreated BMMs (p-value<0.05),
203 which indicates the potential involvement of Bcl-2 in regulating macrophage survival and
204 longevity caused by NP phagocytosis (**Figure 3E**). To further understand the cellular mechanism
205 by which NPs delay rapid apoptosis in *ex vivo* cultures of macrophages, we assessed the expression
206 of B cell lymphoma-extra large (Bcl-xL), which is encoded by the *BCL2-L1* gene and is known to
207 interact with and inhibit executioner caspases 3 and 7 to promote cell survival (**Figure 4E**)[20].
208 Bcl-xL expression was higher in lysates of BMMs treated with 100 µg/ml NPs compared to
209 untreated BMMs, especially at the 3 day timepoint.

210
211 RNAseq analysis and enriched GO terms revealed the involvement of MAPK cascade genes,
212 which are involved in cell function and survival (**Figure 3F**). Notably, we observed the
213 upregulation of *MAP3K11* gene, which has been shown to interact with ERK and other kinases
214 that regulate cell survival[21], and the downregulation of *MAP3K5* gene, which is known for its
215 pro-apoptotic role especially in some disease environments[22, 23]. Guided by RNA sequencing
216 analysis showing the involvement of MAPK cascade in NP-treated cells and the role of MAPK
217 proteins in regulating cell survival and suppressing apoptosis[24], we elected to determine whether
218 proteins in the MAPK cascade are involved in NP-induced macrophage longevity. Analysis of
219 Western blots showed activation of p38 MAPK through increased phosphorylation in NP-treated
220 BMMs compared to their untreated counterparts (**Figure 3G**). In addition, strong phosphorylation

221 of ERK 1 and 2 (MAPK p42 and p44) was revealed by Western blotting in NP-treated BMMs
222 (**Figure 3G**). These results confirm the increased involvement of MAPK cascade kinases and their
223 activation following NP treatment.

224
225 **Phagocytosis and intracellular trafficking to lysosomal membranes is involved in *ex vivo* NP-**
226 **treated macrophages with links to MAPK pathway activation and survival.** NP entry into the
227 cell can occur through several internalization routes, each contributing to different cellular
228 signaling pathways[4]. Uptake of Cy5-labeled NPs in the presence or absence of inhibitors of
229 internalization was assessed kinetically over a 48-hour period (**Figure 4A**). In the absence of
230 inhibitors, approximately 75% of cells were positive for NPs within 24 hours and approximately
231 95% of cells were particle bearing by 48 hours. Pretreatment with anti-CD16/32 antibodies, which
232 block Fc-mediated internalization did not result in considerably lower NP uptake with %NP+ cells
233 closely matching those without the antibodies at 24 and 48 hour timepoints. Incubation with
234 chlorpromazine, an internalization inhibitor especially for clathrin-mediated endocytosis, resulted
235 in moderately lower uptake with 48.7% \pm 2.7% and 87.1% \pm 1.4% NP+ cells at 24 and 48 hours,
236 respectively. A drastic drop in uptake resulted upon pretreatment with cytochalasin D, a potent
237 inhibitor of actin-dependent internalization pathways especially phagocytosis, with 3.1% \pm 0.2%
238 and 11.7% \pm 1.7% NP+ cells at 24 and 48 hours, respectively. These results indicate that actin-
239 dependent internalization and especially phagocytosis was dominant in BMMs treated with
240 PEGDA NPs.

241
242 Enrichment analysis of RNAseq results using DAVID revealed noteworthy involvement of 16
243 lysosomal membrane genes differing between untreated and treated cells (p-value<0.0001)
244 (**Figure 4B**). *CD68* gene was notably upregulated in NP-treated BMMs. *CD68* encodes a
245 transmembrane glycoprotein, which is a member of the lysosomal/endosomal-associated
246 membrane glycoprotein (LAMP) and the scavenger receptor families and is involved in regulating
247 phagocytosis and clearing debris[25]. In addition, *SCARB1* gene was upregulated, suggesting that
248 NPs were phagocytosed by BMMs potentially through scavenger receptors and processed by
249 involving lysosomal compartments. Furthermore, the upregulation of late endosomal/lysosomal
250 adaptor, MAPK and mTOR activator 1 gene (*LAMTOR1*) was noteworthy, suggesting a link
251 between phagocytosis and lysosomal membranes and activation of downstream cell signaling

252 influencing survival. Lysosomal tracking through imaging with LysoBrite™ Green at 24 and 72
253 hours (**Figures 4C, Figure S9**) revealed high intensity regions of lysosomal activity in NP-treated
254 BMMs compared to untreated controls, which may correspond to NP trafficking in late lysosomal
255 compartments. Western blotting for LAMTOR proteins revealed a generally higher expression in
256 NP-treated cells compared to the untreated control (**Figure 4D**). LAMTOR1 and LAMTOR3
257 protein expression was higher in lysates of BMMs treated with 100 µg/ml NPs compared to
258 untreated BMMs especially at the day 1 timepoint. LAMTOR2 expression was consistently higher
259 in NP-treated cells than in untreated cells both at day 1 and day 3 of analysis. Overall, these results
260 strongly suggest that NP phagocytosis and subsequent lysosomal involvement are primary
261 processes involved in cell-particle interactions that ultimately lead to enhancing survival.

262
263 ***In vivo* dosing of NPs and internalization stimulates the lysosome and upregulates pro-**
264 **survival factors.** 100 µg of NPs were dosed to mice via orotracheal instillations and intraperitoneal
265 injections to investigate the *in vivo* implications of NP phagocytosis. Alveolar and peritoneal
266 lavages were performed at 24 hours following administration and CD11b+ macrophages were
267 considered for analysis (Representative flow cytometric gating in **Figure S10**). NP uptake by
268 macrophages was assessed (**Figure 5A**); approximately 83% and 80% of peritoneal and alveolar
269 macrophages, respectively, were determined to be NP+ via flow cytometry. Lysosomal tracking
270 in alveolar and peritoneal macrophages was performed through imaging with LysoBrite™ Green
271 (**Figure S11**) and revealed high intensity regions of lysosomal activity in alveolar and peritoneal
272 macrophages from NP-dosed mice compared to their untreated counterparts, which may be
273 associated with NP trafficking to late lysosomal compartments and subsequent stimulation of
274 lysosomal signaling.

275
276 To investigate whether NP internalization by macrophages *in vivo* has pro-survival implications,
277 anti-apoptotic Bcl-2 expression was evaluated in alveolar and peritoneal macrophages from NP-
278 dosed mice. Flow cytometric analysis of alveolar and peritoneal macrophages from NP-dosed mice
279 (**Figure 5B**) showed a markedly higher Bcl-2 expression in both alveolar and peritoneal
280 macrophages from NP-dosed mice compared to their untreated counterparts. Median fluorescence
281 intensities (MFI) of AlexaFluor488-conjugated anti-Bcl-2 antibodies were 14,870 and 19,262 for
282 peritoneal macrophages from untreated and NP-dosed mice, respectively and 31,305 and 40,004

283 for alveolar macrophages from untreated and NP-dosed mice, respectively, indicating upregulation
284 of anti-apoptotic Bcl-2 upon *in vivo* NP dosing. Immunostaining reveals notably higher expression
285 of Bcl-2 in peritoneal and alveolar macrophages from NP-dosed mice relative to their untreated
286 counterparts, characterized by higher intensity of green fluorescence (**Figure 5C,D**) confirming
287 the results from flow cytometric analyses. Interestingly, TUNEL analysis revealed no notable
288 differences between peritoneal macrophages from untreated and NP-dosed mice (**Figure S12**),
289 indicating low overall apoptotic activity in *in vivo* macrophages despite NP-driven Bcl-2
290 upregulation.

291 292 **DISCUSSION**

293 In this study, we demonstrated that dosing primary macrophages with inert and unfunctionalized
294 NPs results in enhanced *ex vivo* survival for extended periods of time. Survival of macrophages
295 was a strong function of NP concentration and did not rely on traditional activation and
296 polarization pathways, which indicates a unique pro-survival effect in the absence of hallmark
297 TLR stimulation. Macrophages dosed with NPs avoided apoptosis through mechanisms linked
298 with phagocytosis and downstream NP processing in lysosomal compartments. Enhanced
299 macrophage longevity was observed following treatment of a wide range of particle chemistries in
300 BMMs, as well as primary alveolar and peritoneal macrophages, suggesting a universal effect of
301 particle internalization by phagocytes driving cell lifespan. Furthermore, *in vivo* dosing of NPs to
302 mice resulted in upregulation of pro-survival proteins and stimulation of lysosomal activity, in
303 agreement with *ex vivo* results. This work has important implications for understanding and
304 regulating cell lifespan through internalization of any foreign body.

305
306 BMMs are an established *in vitro* primary macrophage model that are differentiated *ex vivo* and
307 are widely used to study macrophage function. BMMs require relatively high amounts of
308 granulocyte-macrophage colony-stimulating factor (GM-CSF) for differentiation and
309 proliferation, yielding high numbers of primary-like macrophage cells. However, BMMs rapidly
310 undergo apoptosis in the absence of GM-CSF stimulating factors[19]. Our results demonstrated
311 that a single dosage of PEGDA NPs in the absence of other signals, including GM-CSF, can
312 dramatically extend their lifespan. In addition, we investigated the effect of NP dosing on the
313 survival of terminally differentiated primary alveolar and peritoneal macrophages *ex vivo*. Our
314 results demonstrated that treatment with PEGDA NPs significantly improved the survival of all

315 the tested macrophage types, indicating that NP-induced survival may extend to a wide range of
316 macrophage populations and phagocytic cells. The identified pathways linking phagocytosis,
317 lysosomal signaling, and cell lifespan are ubiquitous to many phagocytes (**Figure 4E**); thus,
318 similar extended viability would be expected for a wide range of innate immune cells following
319 particulate internalization[26]. While our results have yet to explore additional phagocytes or their
320 extended survival in the *in vivo* environment, we have demonstrated NP-driven upregulation of
321 pro-survival Bcl-2 proteins and stimulation of lysosomal activity following *in vivo* NP dosing,
322 indicating that particulate-induced cell survival may occur *in vivo*. Furthermore, poorly soluble
323 particulate adjuvants (*e.g.*, aluminum hydroxide [alum], talc, oil-in-water emulsions, aggregated
324 oxidized low density lipoproteins [ox-LDL]) have been shown to extend phagocyte survival (*i.e.*,
325 macrophage, dendritic cell) at the site of injection in the absence of GM-CSF[27]. While this
326 extended survival is often attributed to inflammatory signaling cascades or macrophage
327 polarization, our results with non-stimulatory PEGDA NPs suggests survival can be independently
328 promoted through phagocytosis and likely enhanced with inflammatory synergies. Further
329 explorations in other phagocytes and macrophage populations both *ex vivo* and *in vivo* are
330 warranted to continue to decouple these effects.

331
332 Our study leveraged PEGDA hydrogel NPs, commonly used in the drug delivery field to extend
333 circulation times, encapsulate hydrophilic cargos, and evaluate physiochemical NP properties[28,
334 29]. Importantly, PEGDA nanoparticles have been shown to be immunologically inert[30], in
335 contrast to commonly used biodegradable hydrophobic polyesters, such as poly(lactic-co-glycolic
336 acid) (PLGA), that yield acidic degradation products with immunomodulatory effects[31]. Indeed,
337 BMMs treated with PEGDA-NPs showed no evidence of PRR activation (**Figure S5**), allowing us
338 to confirm the effects of NP-induced longevity occur independently from stimulatory signaling
339 pathways. However, the NP-enhanced survival of BMMs was not found to be unique to this
340 formulation; BMMs treated with other unfunctionalized NPs of different compositions all
341 displayed enhanced viability following a single administration. Polystyrene, silica, gold, and silver
342 NPs resulted in significantly higher BMM counts after one week relative to untreated BMMs and
343 were all higher than cell counts of PEGDA NP-treated BMMs. We hypothesize that variable NP
344 uptake contributes to differences in the resulting survival; relative to PEGDA NPs, other NPs are
345 composed of stiffer materials which will promote higher uptake in macrophages[28]. Furthermore,

346 silver, gold, silica, and polystyrene NPs have been shown to cause activation and polarization in
347 macrophages[9], which could also explain differences in survival across nanoparticle types and
348 points to synergize arising from inflammatory and phagocytic cascades. Regardless, the BMM
349 response to the range of NP groups highlight that NP-induced macrophage survival may be
350 universally applicable to NPs of all compositions, emphasizing the broad importance of our
351 findings for the drug delivery community.

352
353 Within 24 hours of GM-CSF depletion, a significant portion of *ex vivo* BMMs transitioned to
354 apoptotic regimes, supported by executioner caspase activity and DNA damage assays (**Figure 3**).
355 Suppression of executioner caspase 3/7 activity is likely due to interactions with anti-apoptotic
356 Bcl-2 family proteins including Bcl-2 and Bcl-xL, which were found to be upregulated in NP-
357 treated *ex vivo* BMMs (**Figure 3**) as well as *in vivo*-dosed alveolar and peritoneal macrophages
358 (**Figure 5**). Anti-apoptotic Bcl-2 family proteins have been known to promote survival through
359 the inhibition of caspase activation in apoptosis signaling[20, 32]. Following phagocytosis, which
360 we confirm is the dominate route of NP internalization (**Figure 4A**), internalized particles are
361 channeled through cellular compartments starting from the phagosome and through the matured
362 phagolysosome, triggering a myriad of signaling pathways[4]. Phagocytosis initiates through a
363 multitude of surface receptors that can generally be grouped into two classes: opsonin-dependent
364 (*i.e.* Fc and complement receptors, integrins) and opsonin-independent (*i.e.* scavenger receptors,
365 c-type lectins)[26]. However, other internalization pathways may be responsible for NP uptake
366 and trafficking including, *e.g.* pinocytosis and endocytosis, which shuttle the internalized NP to
367 the lysosomal compartment. Regardless of the route of entry, the lysosome is a hotspot for
368 signaling and is associated with a wide range of pathways regulating survival, including some
369 MAPK pathway proteins (*e.g.*, ERK1/2) that are intimately intertwined with and regulated by
370 lysosomal activity[33]. Indeed, RNAseq enrichment analysis (**Figure S6**) highlighted the role of
371 MAPK, lysosomal proteins, and protein kinase B in the anti-apoptotic events. ERK1/2 activation
372 has been linked to enhanced survival through the upregulation of anti-apoptotic proteins that
373 belong to the Bcl-2 family (**Figure 4E**)[34]. Our results indicated that LAMTOR1, LAMTOR2,
374 and LAMTOR3 were upregulated in cell lysates of NP-treated BMMs, corresponding to
375 phosphorylation of ERK1/2 and p38 MAPK, in parallel to gene level upregulation of *LAMTOR1*
376 and several genes in the MAPK cascade, which were ultimately reflected in the resulting anti-

377 apoptotic activity. Depletion of lysosomal proteins, especially LAMTOR1 and LAMTOR2, has
378 been shown to cause rapid apoptosis in phagocytes[35, 36], indicating the role of late endosomal
379 and lysosomal cellular compartments in regulating survival. Our reports of increased LAMTOR
380 activity (**Figure 4D**) implicated this family in macrophage resistance to apoptosis following NP
381 phagocytosis. Along with ERK1/2 phosphorylation, protein kinase B and p38 MAPK activation
382 have been shown to be involved in promoting cell survival[37]. Phosphorylation of p38 MAPK
383 revealed an additional route through which NP phagocytosis may influence macrophage survival.
384 Activation of p38 MAPK and its associated pathways has been implicated in apoptosis resistance
385 in monocytes and macrophages[38]. Altogether, this unravels unexplored interactions of
386 phagocytosis and survival signaling that are likely stemming from the involvement of lysosomal
387 signaling.

388
389 Macrophage survival in response to external stimuli has been commonly linked to traditional TLR
390 signaling leading to potent Nuclear Factor (NF)- κ B activation and the transcription of
391 inflammatory genes[39], which results in the secretion of cytokines and ultimately leading to
392 polarization into an inflammatory phenotype. Stimulation of NF- κ B signaling has been previously
393 utilized to prolong the survival of *ex vivo* macrophages and other leukocytes using cytokines[40],
394 TLR agonists,[39] adjuvants[41], and some lipoproteins (ox-LDL)[42]. Similar extension of
395 phagocyte survival has also been attributed to autophagy signaling, with internalization of
396 apoptotic cells promoting phagocyte survival through Protein kinase B (Akt) activation and MAPK
397 ERK1/2 inhibition[43]. Autophagy can also regulate phagocyte activation state through NF- κ B
398 signaling degradation and the mechanistic target of rapamycin (mTOR) pathway, which has been
399 attributed to M1 and M2 polarization[44, 45]. However, owing to the immunologically inert nature
400 of PEG-based materials[30], PEGDA NPs did not lead to macrophage activation or significant
401 changes to inflammatory cytokine secretions, which enabled the decoupling of survival and
402 activation phenomena with respect to understanding the impact of NP phagocytosis on primary
403 macrophage fate. Interestingly, PEGDA NP phagocytosis promoted upregulation of MHCII
404 despite insignificant changes to M1 or M2 activation markers. While MHCII expression
405 traditionally accompanies other polarization markers along the M1-M2 paradigm, including CD86
406 or CD206 in response to polarizing stimuli[46], these were not observed in our results (**Figure**
407 **S5**). Other NP systems have been shown to cause MHCII upregulation, but these reports are often

408 coupled with markers of macrophage polarization[9]. Thus, treating with PEGDA NPs could
409 enhance MHCII expression for vaccine studies, *in vitro* drug screening, or immune-skewing
410 therapeutics without significant impact on phenotypical state. This may be especially critical for
411 developing NP-based tolerizing therapies, where presentation of antigens in the absence of pro-
412 inflammatory stimuli may enhance the tolerogenic effects of the NP therapy, especially for
413 treatment of allergic responses or autoimmune diseases[47].

414
415 The discoveries made in this work outline the strong dependence of macrophage survival on NP
416 phagocytosis in *ex vivo* cultures, which are plagued by rapid apoptosis. These findings are of
417 special importance for improving macrophage utility in drug discovery and screening, as well as
418 biomanufacturing opportunities. Furthermore, autologous macrophage therapies[48], which
419 commonly rely on *ex vivo* stimulation prior to *in vivo* administration will greatly benefit from
420 increased survival throughout the stimulation period of the explant, which may extend to *in vivo*
421 implants. In addition to more certain *ex vivo* survival improvements, the presented findings also
422 indicate potential enhancement of macrophage survival in *in vivo* environments as a result of NP-
423 driven upregulation of anti-apoptotic proteins. Both peritoneal and alveolar macrophages exhibited
424 lysosomal involvement following *in vivo* NP administration that led to increasing Bcl-2 expression
425 (**Figure 5**), in line with *ex vivo* results from these same primary cell types. Interestingly, alveolar
426 macrophages expressed higher basal levels of Bcl-2 when compared to peritoneal macrophages,
427 which may be attributed to differential function, exposure conditions, and lifespans; alveolar
428 macrophages reside at a mucosal interface and can span many months to years[49], while
429 peritoneal macrophages are less exposed to external stimuli and can present both short- and long-
430 half-lives depending on their precursor origin[50]. Regardless, both cell types exhibited increased
431 anti-apoptotic Bcl-2 expression following *in vivo* NP treatment, suggesting NP internalization *in*
432 *vivo* will influence downstream cell viability. Upregulation of anti-apoptotic factors *in vivo*
433 presents unique therapeutic opportunities where pro-apoptotic potential is imposed, for example
434 in the case for some bacterial infections[51], where NP treatment to macrophages may suppress
435 apoptosis and aid in host defense. In the context of drug delivery applications, the fate of NPs
436 following *in vivo* administration is overwhelmingly affected by phagocytes, especially
437 macrophages[4], NP interactions with phagocyte survival must be studied in drug delivery systems
438 especially where macrophages may play a crucial role in the pathology, as is the case with

439 atherosclerosis[52], asthma[53], or idiopathic pulmonary fibrosis[54]. Long-term studies are
440 needed to uncover what, if any, negative effect increased survival may have on other cell
441 functionality. Thus, thorough investigations of NP interactions with macrophages and other
442 phagocytes are critical to understanding of the role of phagocytes in healthy and disease conditions
443 and, ultimately, NP therapeutic employment.

444
445 Altogether, enhancing survival of macrophages leveraging NP platforms opens the door to a wide
446 range of opportunities in therapeutic interventions with implications in drug delivery, drug
447 screening, cell therapies, immune engineering. Furthermore, these results aid to decouple the
448 mechanisms involved in phagocytosis pathways that regulate cell viability to promote predictive
449 understanding of phagocyte lifespan both *ex vivo* and *in vivo*.

450

451 **METHODS**

452 Primary Macrophage Isolation and Murine Studies

453 All studies involving animals were performed in accordance with National Institutes of Health
454 guidelines for the care and use of laboratory animals and approved by the Institutional Animal
455 Care and Use Committee (IACUC) at the University of Delaware. C57BL/6J (Jackson
456 Laboratories) were housed in a pathogen-free facility at the University of Delaware. Female
457 C57BL/6J six to ten weeks of age were used to extract primary cells. BMMs and alveolar and
458 peritoneal macrophages were isolated from mice according to standard protocols as described in
459 the following.

460

461 To generate bone marrow-derived macrophages (BMMs), standard protocols as previously
462 reported were followed[55]. Briefly, bone marrow was extracted from femurs and tibias of mice
463 following euthanasia and cells were plated in BMM differentiation media (DMEM/F-12 media
464 (Corning) containing 20% fetal bovine serum, 30% L929 cell conditioned media, and 1%
465 Penicillin-Streptomycin). On day three, cells were supplemented with an additional dose of BMM
466 differentiation media and used on day seven for experiments following removal of L929 cell
467 conditioned media and culture in DMEM/F-12 media containing 10% fetal bovine serum.

468

469 For *in vivo* studies, 100 μg NPs in PBS were administered to mice to the lungs via an orotracheal
470 instillation or to the peritoneal cavity via an intraperitoneal injection according to standard
471 methods. Primary alveolar macrophages were extracted from mice by performing a
472 bronchoalveolar lavage (BAL) and extracting the BAL fluid (BALF). Briefly, BALF was spun
473 down in a cold centrifuge at 1500 rpm for five minutes and the cell pellet was resuspended in red
474 blood cell lysis buffer (Invitrogen) for 60 seconds and then resuspended in DMEM/F-12 media
475 containing 10% fetal bovine serum, and 1% Penicillin-Streptomycin and seeded in well plates for
476 experiments. Primary peritoneal macrophages were isolated from mice by performing a peritoneal
477 lavage (PL) and extracting the PL fluid (PLF) as previously described[55]. The PLF was spun
478 down in a cold centrifuge at 1500 rpm for 5 minutes and the cell pellet was resuspended in
479 DMEM/F-12 media containing 10% fetal bovine serum, and 1% Penicillin-Streptomycin and
480 plated in well plates overnight to allow for peritoneal macrophages to adhere. Following overnight
481 incubation, nonadherent cells were removed and cells were scraped and re-plated for experiments.

482

483 NP Synthesis

484 Poly(ethylene glycol) diacrylate (PEGDA)-based NPs were synthesized as previously
485 described[56]. Briefly, PEG₇₀₀DA ($M_n = 700$), 2-carboxyethyl acrylate (CEA), and photoinitiator
486 diphenyl(2,4,6-trimethylbenzoyl) phosphine oxide were dissolved in methanol (50wt% solution)
487 and emulsified with silicone oil AP1000 (All from Millipore Sigma) (**Figure S1**) and polymerized
488 by irradiating with UV light (365 nm at ~ 28 cm from the light source, $\sim 5\text{--}10$ mW/cm²) for the 30
489 seconds. Micron-sized particles were eliminated by passing the suspension through a series of
490 sterile five-micron and one-micron filters. The resulting NPs were washed twice in sterile water
491 prior to a final suspension in DMEM/F-12 media containing 10% fetal bovine serum, and 1%
492 Penicillin-Streptomycin for use in experiments. In experiments requiring particle tracking, FITC
493 (Millipore Sigma) or Cy5 maleimide (AAT Bioquest) fluorescent labels were included in the
494 monomer mix at compositions of 1% and 0.25%, respectively. In experiments with non-PEGDA
495 NPs, unfunctionalized 100 nm silver, gold, and silica NPs (Nanocomposix) as well as 100 nm
496 polystyrene NPs (Millipore Sigma) were obtained.

497

498

499

500 NP Characterization

501 Thermogravimetric analysis (TGA) using TA Instruments TGA 550 was utilized to determine NP
502 concentrations following the final water wash. 50 µl of NP suspensions were added to TGA sample
503 pans in technical triplicates at a series of dilutions. The mass of the NPs was determined via a mass
504 reading after a temperature ramp to 120 °C followed by a 30-minute isothermal step to ensure
505 water evaporation. Dynamic light scattering (DLS) was performed using a Malvern Zetasizer Nano
506 S to characterize the hydrodynamic diameter of NPs. NPs were prepared for DLS by diluting to
507 0.1 mg/ml in deionized water. Hydrodynamic diameters and polydispersity indices were measured
508 for technical triplicates. Scanning electron microscopy (SEM) was performed using a JSM F7400
509 scanning electron microscope following gold/palladium sputter coating using a Denton Desk IV
510 sputter coater. Endotoxin contamination was assessed for all NP groups using Pierce™ LAL
511 Chromogenic Endotoxin Quantitation Kit (ThermoFisher Scientific) according to manufacturer's
512 guidelines.

513

514 NP Internalization and Trafficking

515 BMMs were seeded in 24-well plates (2.5×10^5 cells/well) and allowed to adhere for at least four
516 hours prior to NP treatment. NPs were administered to cells at the indicated final concentrations
517 for 24 hours. Kinetic NP uptake was determined by dosing BMMs with 100 µg/ml Cy5-labelled
518 NPs. Cells were detached using Accutase® (Innovative Cell Technologies, Inc.) at 0, 4, 8, 16, 24,
519 and 48 hours and analyzed for %Cy5+ cells using ACEA NovoCyte Flow Cytometer. To
520 differentiate internalization pathways, BMMs were treated with 2 µg/ml anti-CD16/32, 1.5 µg/ml
521 Cytochalasin D, or 5 µg/ml Chlorpromazine hydrochloride 30 minutes prior to NP dosing and
522 analyzed at 0, 4, 8, 16, 24, and 48 hours following NP treatment for %Cy5+ cells using Flow
523 Cytometry. For lysosomal imaging, cells were cultured in glass bottom, black walled 96-well
524 plates ($0.5-1.5 \times 10^4$ cells/well) and Cell Navigator™ Lysosome Staining Kit (AAT Bioquest) was
525 used according to manufacturer's guidelines. Cells were imaged using BioTek Cytation 5
526 Multimode Imager.

527

528 Cell Viability Assessment

529 BMMs were seeded in 96-well plates (1×10^5 cells/well) and allowed to adhere for at least four
530 hours prior to NP treatment. NPs were administered to cells at the indicated concentrations for 24

531 hours. Metabolic activity as a measure of cell viability was assessed using CellTiter-Glo® 2.0 Cell
532 Viability Assay (Promega) according to manufacturer's guidelines. BioTek Cytation 5 Multimode
533 Imager was also used to monitor cell counts as a measure of viability. Zombie Yellow™ Fixable
534 Viability Kit (Biolegend) was used according to manufacturer's guidelines for flow cytometric
535 assessment of cell viability. For apoptosis detection, Caspase-Glo® 3/7 Assay System (Promega)
536 was used according to manufacturer's guidelines. Phosphatidylserine membrane translocation was
537 quantified using fluorescent staining with Annexin V-Pacific Blue (Biolegend). Bcl-2 anti-
538 apoptotic protein expression was measured by intracellular staining of BMMs with PE-Cy7 anti-
539 Bcl-2 antibody (Biolegend). AlexaFluor488 anti-Bcl-2 and BV711 anti-CD11b antibodies
540 (Biolegend) were used for staining of *in vivo* NP-treated alveolar and peritoneal macrophages. For
541 TUNEL assay, cells were cultured in glass bottom, black walled 96-well plates ($0.5-1.5 \times 10^4$
542 cells/well) and Cell Meter™ Live Cell TUNEL Apoptosis Assay Kit (AAT Bioquest) was used
543 according to manufacturer's guidelines. Gene and protein analysis of NP-treated BMMs is
544 described in the following sections.

545

546 Western Blotting

547 BMMs were seeded in 6-well plates (1×10^6 cells/well) and allowed to adhere for at least four hours
548 prior to NP treatment. NPs were administered to cells at the indicated final concentrations for 24
549 hours. BMMs were harvested and lysed with ice-cold RIPA lysis buffer (Alfa Aesar) supplemented
550 with Halt Protease and Phosphatase Inhibitors (ThermoFisher Scientific). Cell lysates were spun
551 down at 16,000 RCF for ten minutes in a precooled centrifuge and supernatants were collected.
552 Protein content of supernatants was determined using a BCA assay (ThermoFisher Scientific).
553 Following denaturation of protein samples in Laemmli sample buffer (Bio-Rad), 15 µg of protein
554 were loaded onto 4-20% Mini PROTEAN gels (Bio-Rad) and run at 50 V for five minutes followed
555 by 150 V for 60 minutes in running buffer (25 mM Tris, 192 mM glycine, and 0.1% SDS, pH 8.3).
556 Protein bands were transferred to PVDF membranes (Bio-Rad) and blocked for two hours with
557 5% bovine serum albumin (BSA) in Tris-buffered saline with 0.1% Tween20 (TBST) and
558 incubated overnight in Bcl-xL, p44/42 MAPK (ERK1/2), phospho- p44/42 MAPK (ERK1/2)
559 (Thr202/Tyr204), GAPDH, LAMTOR1, LAMTOR2, LAMTOR3, p38 MAPK, phospho-p38
560 MAPK(Thr180/Tyr182) anti-mouse primary antibodies diluted according to manufacturer's
561 guidelines in TBST containing 5% BSA. Membranes were then washed three times in TBST and

562 incubated with horseradish peroxidase-conjugated anti-Rabbit IgG secondary antibody (All
563 antibodies from Cell Signaling Technology) at 1:2000 dilution in TBST containing 5% BSA.
564 Membranes were then washed three times in TBST prior to incubation with Amersham
565 Chemiluminescent Detection Set (GE Healthcare) for visualization. Membranes were imaged
566 using Azure 280 Imager. Each membrane was reserved for each primary antibody and all the
567 reported blots are from the same batch of lysates; housekeeping protein (GAPDH) was blotted
568 independently for the same batch of lysates.

569

570 Macrophage Polarization Studies

571 BMMs in 6-well plates (1×10^6 cells/well) were detached using Accutase® (Innovative Cell
572 Technologies, Inc.) and washed twice with PBS supplemented with 2% FBS. Cells were then
573 blocked with anti-CD16/32 (Fc block, Biolegend) for 10 minutes and then surface-stained for 30
574 minutes with the following antibodies: CD38-Pacific Blue, CD86-AlexaFluor700, and I-A/I-E-
575 Brilliant Violet 785™ (All from Biolegend). Cells were then fixed with 4% paraformaldehyde in
576 PBS (Alfa Aesar) for 15 minutes and then permeabilized using Intracellular Staining
577 Permeabilization Wash Buffer (Biolegend) and stained for intracellular markers with the following
578 antibodies: CD206-PE-Cy7 and EGR2-APC (All from Biolegend) and analyzed using ACEA
579 NovoCyte Flow Cytometer. Median fluorescent intensity (MFI) was recorded via flow cytometry
580 as a measure of marker expression. In some studies, 25 ng/ml lipopolysaccharides (LPS) from
581 *Escherichia coli* O111:B4 (Millipore Sigma) or 25 ng/ml Interleukin-4 (IL-4) (Biolegend) were
582 used to stimulate M1 or M2 polarization, respectively for 24 hours prior to use in experiments. For
583 cytokine analyses, concentrations of supernatant at no dilution were measured in BMM
584 supernatants by the Cytokine Core Laboratory at the University of Maryland (Baltimore) for
585 Eotaxin, G-CSF, GM-CSF, IFN- γ , IL-1 α , IL-1 β , IL-2, IL-3, IL-4, IL-5, IL-6, IL-7, IL-9, IL-10,
586 IL-12 p40, IL-12 p70, IL-13, IL-15, IL-17 α , IP-10, KC, LIF, LIX, MCP-1, MCSF, MIG, MIP-1 α ,
587 MIP-1 β , MIP-2, RANTES, TNF- α , and VEGF- α using a 32-panel LUMINEX multianalyte
588 system. Enzyme-Linked Immunosorbent Assays (ELISAs) kits (BD Biosciences) for Interleukin-
589 6 (IL-6) and Tumor Necrosis Factor- α (TNF- α) were also performed on BMM supernatants
590 according to manufacturer's guidelines.

591

592

593 RNA Sequencing and Bioinformatics

594 BMMs were seeded in 6-well plates (1×10^6 cells/well) and allowed to adhere for at least four hours
595 prior to NP treatment. NPs were administered to cells at the indicated final concentrations for 24
596 hours. BMMs were lysed *in situ* and RNA was extracted and purified using RNAeasy Plus Mini
597 Kit (Qiagen) according to manufacturer's guidelines. RNA samples were sequenced by the
598 University of Delaware Sequencing and Genotyping Center at the Delaware Biotechnology
599 Institute. Libraries were prepared using Perkin Elmer NEXTflex Rapid Directional RNA-seq V1
600 following the manufacturer's instructions. Library quality analysis was performed by digital
601 droplet PCR. Sequencing was performed on Illumina NextSeq 550 platform using a NextSeq v2.5
602 75-cycle high output kit as per the manufacturer's instructions. Raw sequence data was analyzed
603 by the Center for Bioinformatics and Computational Biology Core Facility at the University of
604 Delaware using the established RNAseq analysis pipeline (adapted from Kalari *et al.*[57]). Quality
605 of sequencing data was assessed using FastQC (ver. 0.10.1; Babraham Bioinformatics). Reads
606 were trimmed for quality ($Q < 30$) and to remove poly-A and Illumina sequencing adapters using
607 Trim Galore! (ver. 0.4.4; Babraham Bioinformatics) and reads less than 35bp after trimming were
608 discarded, resulting in 495.5M quality reads (per sample mean: 41.3M; range: 35.36-45.46M).
609 Trimmed reads were aligned to the *M. musculus* genome (version mm10) using HiSat2[58] (ver.
610 2.1.0; mean mapping rate 95.5%), mapping metrics were assessed using RseQC[59] (ver. 2.6.1),
611 and gene/exon feature counts were calculated using HTseq[60] (ver. 0.11.0). Pairwise differential
612 expression analysis was performed to identify gene-level features which are significantly up or
613 down-regulated between treatments using EdgeR[61, 62] (ver. 3.28.1) analyzing genes with a
614 CPM (count per million reads) of at least one in three or more samples. Database for Annotation,
615 Visualization and Integrated Discovery (DAVID)[63, 64] was used to perform GO enrichment
616 analysis and functional classifications.

617

618 Statistical analysis

619 GraphPad Prism 8 (GraphPad Software Inc) was used to perform statistical analysis. All
620 quantitative data are represented as mean \pm standard deviation (SD) or standard error of the mean
621 (SEM). Data shown are from representative results from at least two independent experiments,
622 with the exception of RNAseq data. Tukey's or Dunnett's multiple-comparison test or Student's
623 T-test were used to generate p-values in ANOVA multiple comparisons, unless stated otherwise.

624 **DATA AVAILABILITY**

625 RNAseq data is submitted to Gene Expression Omnibus (GEO) public repository and data can be
626 accessed through accession number GSE161941.

627 **ACKNOWLEDGEMENTS**

628 The authors acknowledge J.D. Bhavsar and S.W. Polson for Bioinformatics assistance and B.
629 Kingham for RNA sequencing assistance. The authors also thank W. Chen, A. Kunjapur for
630 Western blotting assistance and access to imager in addition to G. Robbins, J. DeSimone for
631 helpful conversations. BioRender.com was used to create sketches.

632

633 **AUTHOR CONTRIBUTIONS**

634 B.M.J., C.A.F. designed research; B.M.J. performed experiments; B.M.J., C.A.F. analyzed data
635 and wrote the paper.

636

637 **COMPETING INTERESTS**

638 No competing interests exist.

639

640 **FUNDING INFORMATION**

641 Research reported in this publication was supported by the National Institutes of Health and the
642 State of Delaware under Award Number P20GM103446 and P20GM104316, as well as a Research
643 Starter Grant in Pharmaceuticals from the PhRMA Foundation, and a University of Delaware
644 Research Foundation Award. The content is solely the responsibility of the authors and does not
645 necessarily represent the official views of the National Institutes of Health.

646 **REFERENCES**

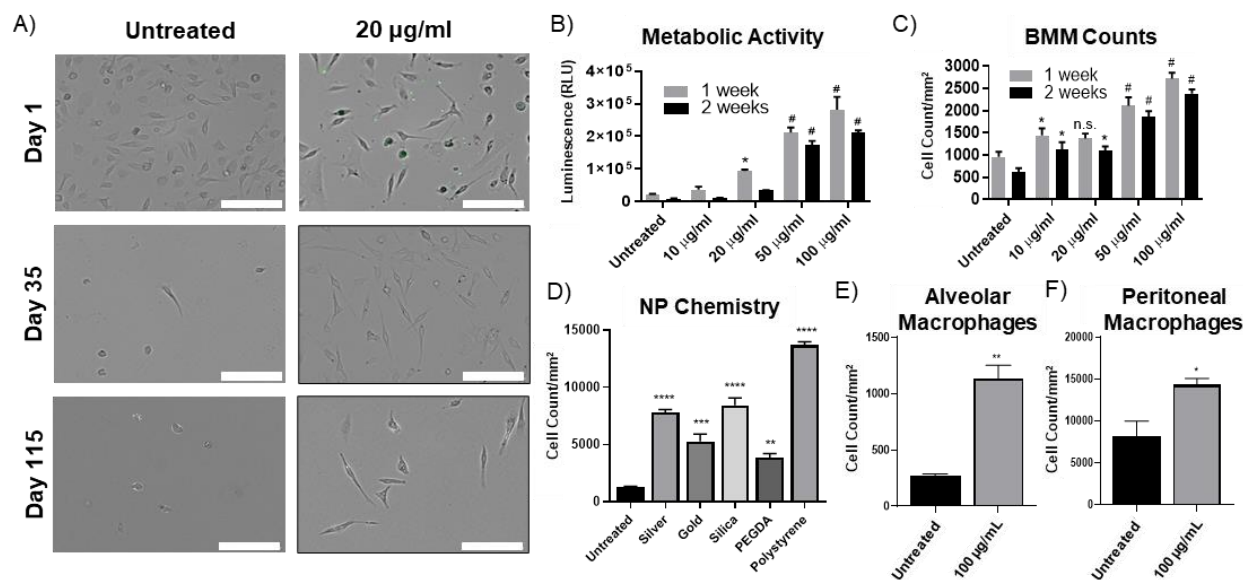
- 647 1. Gordon, S.; Plüddemann, A., Tissue macrophages: Heterogeneity and functions. *BMC*
648 *Biol*, **2017**; Vol. 15.
- 649 2. Underhill, D. M.; Goodridge, H. S., *Nat Rev Immunol* **2012**, *12* (7), 492-502. DOI
650 10.1038/nri3244.
- 651 3. Irvine, D. J.; Hanson, M. C.; Rakhra, K.; Tokatlian, T., *Chem Rev* **2015**, *115* (19), 11109-
652 11146. DOI 10.1021/acs.chemrev.5b00109.
- 653 4. Gustafson, H. H.; Holt-Casper, D.; Grainger, D. W.; Ghandehari, H., Nanoparticle uptake:
654 The phagocyte problem. **2015**.
- 655 5. Nel, A. E.; Mädler, L.; Velegol, D.; Xia, T.; Hoek, E. M. V.; Somasundaran, P.; Klaessig,
656 F.; Castranova, V.; Thompson, M., *Nature Materials* **2009**, *8* (7), 543-557. DOI
657 10.1038/nmat2442.
- 658 6. Champion, J. A.; Mitragotri, S., *Proc. Natl. Acad. Sci. U. S. A.* **2006**, *103* (13), 4930. DOI
659 10.1073/pnas.0600997103.
- 660 7. Feng, Q.; Liu, Y.; Huang, J.; Chen, K.; Huang, J.; Xiao, K., *Scientific Reports* **2018**. DOI
661 10.1038/s41598-018-19628-z.
- 662 8. Jarai, B. M.; Stillman, Z.; Attia, L.; Decker, G. E.; Bloch, E. D.; Fromen, C. A., *ACS*
663 *Applied Materials & Interfaces* **2020**, *12* (35), 38989-39004. DOI 10.1021/acsami.0c10900.
- 664 9. Reichel, D.; Tripathi, M.; Perez, J. M., Biological effects of nanoparticles on macrophage
665 polarization in the tumor microenvironment. **2019**.
- 666 10. Suk, J. S.; Xu, Q.; Kim, N.; Hanes, J.; Ensign, L. M., PEGylation as a strategy for
667 improving nanoparticle-based drug and gene delivery. **2016**.
- 668 11. Jarai, B. M.; Kolewe, E. L.; Stillman, Z. S.; Raman, N.; Fromen, C. A., Chapter 18 -
669 Polymeric Nanoparticles. In *Nanoparticles for Biomedical Applications*, Chung, E. J.; Leon, L.;
670 Rinaldi, C., Eds. Elsevier: 2020; pp 303-324.
- 671 12. Wilhelm, S.; Tavares, A. J.; Dai, Q.; Ohta, S.; Audet, J.; Dvorak, H. F.; Chan, W. C. W.,
672 *Nature Reviews Materials* **2016**, *1* (5), 16014. DOI 10.1038/natrevmats.2016.14.
- 673 13. Fromen, C. A.; Kelley, W. J.; Fish, M. B.; Adili, R.; Noble, J.; Hoenerhoff, M. J.; Holinstat,
674 M.; Eniola-Adefeso, O., *ACS Nano* **2017**, *11* (11), 10797-10807. DOI 10.1021/acsnano.7b03190.

- 675 14. Wofford, K. L.; Cullen, D. K.; Spiller, K. L., *Journal of Biomedical Materials Research*
676 *Part A* **2019**, *107* (6), 1213-1224. DOI <https://doi.org/10.1002/jbm.a.36617>.
- 677 15. Lewis, J. S.; Stewart, J. M.; Marshall, G. P.; Carstens, M. R.; Zhang, Y.; Dolgova, N. V.;
678 Xia, C.; Brusko, T. M.; Wasserfall, C. H.; Clare-Salzler, M. J.; Atkinson, M. A.; Keselowsky, B.
679 G., *ACS Biomaterials Science & Engineering* **2019**, *5* (5), 2631-2646. DOI
680 10.1021/acsbiomaterials.9b00332.
- 681 16. Saito, E.; Kuo, R.; Pearson, R. M.; Gohel, N.; Cheung, B.; King, N. J. C.; Miller, S. D.;
682 Shea, L. D., *J Control Release* **2019**, *300*, 185-196. DOI 10.1016/j.jconrel.2019.02.025.
- 683 17. Casey, L. M.; Kakade, S.; Decker, J. T.; Rose, J. A.; Deans, K.; Shea, L. D.; Pearson, R.
684 M., *Biomaterials* **2019**, *218*, 119333. DOI <https://doi.org/10.1016/j.biomaterials.2019.119333>.
- 685 18. Safari, H.; Kelley, W. J.; Saito, E.; Kaczorowski, N.; Carethers, L.; Shea, L. D.; Eniola-
686 Adefeso, O., *Science Advances* **2020**, *6* (24), eaba1474. DOI 10.1126/sciadv.aba1474.
- 687 19. Tushinski, R. J.; Oliver, I. T.; Guilbert, L. J.; Tynan, P. W.; Warner, J. R.; Stanley, E. R.,
688 *Cell* **1982**. DOI 10.1016/0092-8674(82)90376-2.
- 689 20. Clem, R. J.; Cheng, E. H. Y.; Karp, C. L.; Kirsch, D. G.; Ueno, K.; Takahashi, A.; Kastan,
690 M. B.; Griffin, D. E.; Earnshaw, W. C.; Veluona, M. A.; Hardwick, J. M., *Proceedings of the*
691 *National Academy of Sciences of the United States of America* **1998**. DOI 10.1073/pnas.95.2.554.
- 692 21. Chadee, D. N.; Kyriakis, J. M., *Nature Cell Biology* **2004**. DOI 10.1038/ncb1152.
- 693 22. Pressinotti, N. C.; Klocker, H.; Schäfer, G.; Luu, V. D.; Ruschhaupt, M.; Kuner, R.;
694 Steiner, E.; Poustka, A.; Bartsch, G.; Sülthmann, H., *Molecular Cancer* **2009**. DOI 10.1186/1476-
695 4598-8-130.
- 696 23. Iriyama, T.; Takeda, K.; Nakamura, H.; Morimoto, Y.; Kuroiwa, T.; Mizukami, J.; Umeda,
697 T.; Noguchi, T.; Naguro, I.; Nishitoh, H.; Saegusa, K.; Tobiume, K.; Homma, T.; Shimada, Y.;
698 Tsuda, H.; Aiko, S.; Imoto, I.; Inazawa, J.; Chida, K.; Kamei, Y.; Kozuma, S.; Taketani, Y.;
699 Matsuzawa, A.; Ichijo, H., *EMBO Journal* **2009**. DOI 10.1038/emboj.2009.32.
- 700 24. Junttila, M. R.; Li, S.-P.; Westermarck, J., *The FASEB Journal* **2008**, *22* (4), 954-965. DOI
701 10.1096/fj.06-7859rev.
- 702 25. Chistiakov, D. A.; Killingsworth, M. C.; Myasoedova, V. A.; Orekhov, A. N.; Bobryshev,
703 Y. V., *Laboratory Investigation* **2017**. DOI 10.1038/labinvest.2016.116.
- 704 26. Linehan, E.; Fitzgerald, D. C., *Eur J Microbiol Immunol (Bp)* **2015**, *5* (1), 14-24. DOI
705 10.1556/eujmi-d-14-00035.

- 706 27. Hamilton, J. A., *Journal of Leukocyte Biology* **2003**, 73 (6), 702-712. DOI
707 <https://doi.org/10.1189/jlb.0103037>.
- 708 28. Anselmo, A. C.; Zhang, M.; Kumar, S.; Vogus, D. R.; Menegatti, S.; Helgeson, M. E.;
709 Mitragotri, S., *ACS Nano* **2015**. DOI 10.1021/acsnano.5b00147.
- 710 29. Fromen, C. A.; Rahhal, T. B.; Robbins, G. R.; Kai, M. P.; Shen, T. W.; Luft, J. C.;
711 DeSimone, J. M., *Nanomedicine: Nanotechnology, Biology and Medicine* **2016**, 12 (3), 677-687.
712 DOI <https://doi.org/10.1016/j.nano.2015.11.002>.
- 713 30. Roberts, R. A.; Shen, T.; Allen, I. C.; Hasan, W.; DeSimone, J. M.; Ting, J. P. Y., *PLOS*
714 *ONE* **2013**, 8 (4), e62115. DOI 10.1371/journal.pone.0062115.
- 715 31. Allen, R. P.; Bolandparvaz, A.; Ma, J. A.; Manickam, V. A.; Lewis, J. S., *ACS Biomater.*
716 *Sci. Eng.* **2018**, 4 (3), 900-918. DOI 10.1021/acsbio.7b00831.
- 717 32. Kluck, R. M.; Bossy-Wetzell, E.; Green, D. R.; Newmeyer, D. D., *Science* **1997**. DOI
718 10.1126/science.275.5303.1132.
- 719 33. Zhou, P.; Yang, X.-L.; Wang, X.-G.; Hu, B.; Zhang, L.; Zhang, W.; Si, H.-R.; Zhu, Y.; Li,
720 B.; Huang, C.-L.; Chen, H.-D.; Chen, J.; Luo, Y.; Guo, H.; Jiang, R.-D.; Liu, M.-Q.; Chen, Y.;
721 Shen, X.-R.; Wang, X.; Zheng, X.-S.; Zhao, K.; Chen, Q.-J.; Deng, F.; Liu, L.-L.; Yan, B.; Zhan,
722 F.-X.; Wang, Y.-Y.; Xiao, G.-F.; Shi, Z.-L., *Nature* **2020**, 579 (7798), 270-273. DOI
723 10.1038/s41586-020-2012-7.
- 724 34. Parihar, A.; Eubank, T. D.; Doseff, A. I., *J Innate Immun* **2010**, 2 (3), 204-215. DOI
725 10.1159/000296507.
- 726 35. Malek, M.; Guillaumot, P.; Huber, A. L.; Lebeau, J.; Pétrilli, V.; Kfoury, A.; Mikaelian, I.;
727 Renno, T.; Manié, S. N., *Cell Death and Disease* **2012**. DOI 10.1038/cddis.2012.39.
- 728 36. Sparber, F.; Scheffler, J. M.; Amberg, N.; Tripp, C. H.; Heib, V.; Hermann, M.; Zahner, S.
729 P.; Clausen, B. E.; Reizis, B.; Huber, L. A.; Stoitzner, P.; Romani, N., *Blood* **2014**. DOI
730 10.1182/blood-2013-08-518555.
- 731 37. Wang, Y.; Zeigler, M. M.; Lam, G. K.; Hunter, M. C.; Eubank, T. D.; Khramtsov, V. V.;
732 Tridandapani, S.; Sen, C. K.; Marsh, C. B., *American Journal of Respiratory Cell and Molecular*
733 *Biology* **2007**. DOI 10.1165/rcmb.2006-0165OC.
- 734 38. Rijal, D.; Ariana, A.; Wight, A.; Kim, K.; Alturki, N. A.; Aamir, Z.; Ametepe, E. S.;
735 Korneluk, R. G.; Tiedje, C.; Menon, M. B.; Gaestel, M.; McComb, S.; Sad, S., *J Biol Chem* **2018**,
736 293 (30), 11913-11927. DOI 10.1074/jbc.RA118.003614.

- 737 39. Lombardo, E.; Alvarez-Barrientos, A.; Maroto, B.; Boscá, L.; Knaus, U. G., *The Journal*
738 *of Immunology* **2007**, *178* (6), 3731. DOI 10.4049/jimmunol.178.6.3731.
- 739 40. Tushinski, R. J.; Stanley, E. R., *Journal of Cellular Physiology* **1983**, *116* (1), 67-75. DOI
740 10.1002/jcp.1041160111.
- 741 41. Hamilton, J. A.; Byrne, R.; Whitty, G., *Journal of Leukocyte Biology* **2000**, *67* (2), 226-
742 232. DOI <https://doi.org/10.1002/jlb.67.2.226>.
- 743 42. Hundal, R. S.; Gómez-Muñoz, A.; Kong, J. Y.; Salh, B. S.; Marotta, A.; Duronio, V.;
744 Steinbrecher, U. P., *Journal of Biological Chemistry* **2003**, *278* (27), 24399-24408.
- 745 43. Reddy, S. M.; Hsiao, K. H. K.; Abernethy, V. E.; Fan, H.; Longacre, A.; Lieberthal, W.;
746 Rauch, J.; Koh, J. S.; Levine, J. S., *The Journal of Immunology* **2002**, *169* (2), 702. DOI
747 10.4049/jimmunol.169.2.702.
- 748 44. Kim, Y. C.; Guan, K.-L., *The Journal of Clinical Investigation* **2015**, *125* (1), 25-32. DOI
749 10.1172/JCI73939.
- 750 45. Wu, M.-Y.; Lu, J.-H., *Cells* **2019**, *9* (1), 70. DOI 10.3390/cells9010070.
- 751 46. Mantovani, A.; Sica, A.; Sozzani, S.; Allavena, P.; Vecchi, A.; Locati, M., *Trends in*
752 *Immunology* **2004**, *25* (12), 677-686. DOI <https://doi.org/10.1016/j.it.2004.09.015>.
- 753 47. Gammon, J. M.; Jewell, C. M., *Advanced Healthcare Materials* **2019**, *8* (4), 1801419. DOI
754 10.1002/adhm.201801419.
- 755 48. Lee, S.; Kivimäe, S.; Dolor, A.; Szoka, F. C., *J Control Release* **2016**, *240*, 527-540. DOI
756 10.1016/j.jconrel.2016.07.018.
- 757 49. Murphy, J.; Summer, R.; Wilson, A. A.; Kotton, D. N.; Fine, A., *American Journal of*
758 *Respiratory Cell and Molecular Biology* **2008**, *38* (4), 380-385. DOI 10.1165/rcmb.2007-0224RC.
- 759 50. Bain, C. C.; Hawley, C. A.; Garner, H.; Scott, C. L.; Schridde, A.; Steers, N. J.; Mack, M.;
760 Joshi, A.; Guilliams, M.; Mowat, A. M. I.; Geissmann, F.; Jenkins, S. J., *Nature Communications*
761 **2016**, *7* (1), ncomms11852. DOI 10.1038/ncomms11852.
- 762 51. Weinrauch, Y.; Zychlinsky, A., *Annual Review of Microbiology* **1999**, *53* (1), 155-187.
763 DOI 10.1146/annurev.micro.53.1.155.
- 764 52. Seimon, T.; Tabas, I., *J Lipid Res* **2009**, *50* Suppl (Suppl), S382-S387. DOI
765 10.1194/jlr.R800032-JLR200.

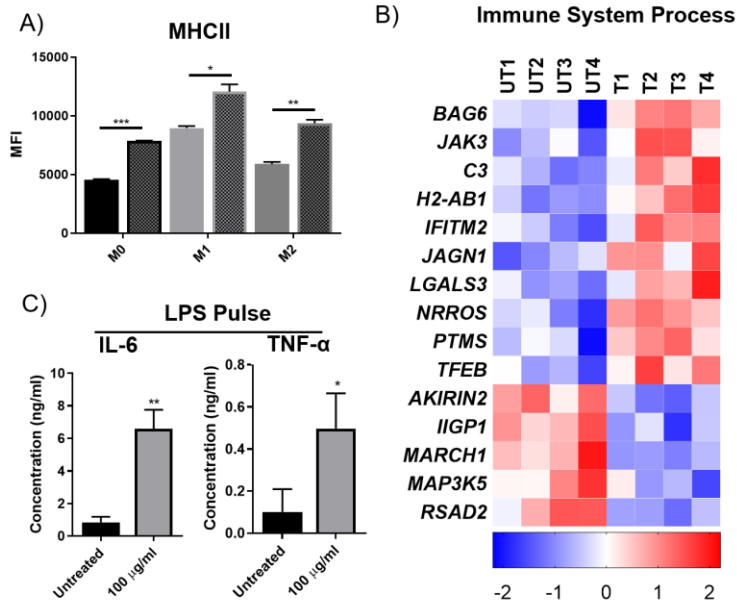
- 766 53. Balhara, J.; Gounni, A. S., *Mucosal Immunology* **2012**, 5 (6), 605-609. DOI
767 10.1038/mi.2012.74.
- 768 54. Byrne, A. J.; Maher, T. M.; Lloyd, C. M., *Trends in Molecular Medicine* **2016**, 22 (4), 303-
769 316. DOI 10.1016/j.molmed.2016.02.004.
- 770 55. Zhang, X.; Goncalves, R.; Mosser, D. M., *Current protocols in immunology* **2008**, Chapter
771 14, Unit-14.1. DOI 10.1002/0471142735.im1401s83.
- 772 56. Stillman, Z.; Jarai, B. M.; Raman, N.; Patel, P.; Fromen, C. A., *Polymer Chemistry* **2020**,
773 11 (2), 568-580. DOI 10.1039/C9PY01206K.
- 774 57. Kalari, K. R.; Nair, A. A.; Bhavsar, J. D.; O'Brien, D. R.; Davila, J. I.; Bockol, M. A.; Nie,
775 J.; Tang, X.; Baheti, S.; Doughty, J. B.; Middha, S.; Sicotte, H.; Thompson, A. E.; Asmann, Y.
776 W.; Kocher, J.-P. A., *BMC Bioinformatics* **2014**, 15 (1), 224. DOI 10.1186/1471-2105-15-224.
- 777 58. Kim, D.; Langmead, B.; Salzberg, S. L., *Nature Methods* **2015**, 12 (4), 357-360. DOI
778 10.1038/nmeth.3317.
- 779 59. Wang, L.; Wang, S.; Li, W., *Bioinformatics* **2012**, 28 (16), 2184-2185. DOI
780 10.1093/bioinformatics/bts356.
- 781 60. Anders, S.; Pyl, P. T.; Huber, W., *Bioinformatics (Oxford, England)* **2015**, 31 (2), 166-169.
782 DOI 10.1093/bioinformatics/btu638.
- 783 61. Robinson, M. D.; McCarthy, D. J.; Smyth, G. K., *Bioinformatics (Oxford, England)* **2010**,
784 26 (1), 139-140. DOI 10.1093/bioinformatics/btp616.
- 785 62. Anders, S.; McCarthy, D. J.; Chen, Y.; Okoniewski, M.; Smyth, G. K.; Huber, W.;
786 Robinson, M. D., *Nature Protocols* **2013**, 8 (9), 1765-1786. DOI 10.1038/nprot.2013.099.
- 787 63. Huang, D. W.; Sherman, B. T.; Lempicki, R. A., *Nature Protocols* **2009**. DOI
788 10.1038/nprot.2008.211.
- 789 64. Huang, D. W.; Sherman, B. T.; Lempicki, R. A., *Nucleic Acids Research* **2009**. DOI
790 10.1093/nar/gkn923.
791



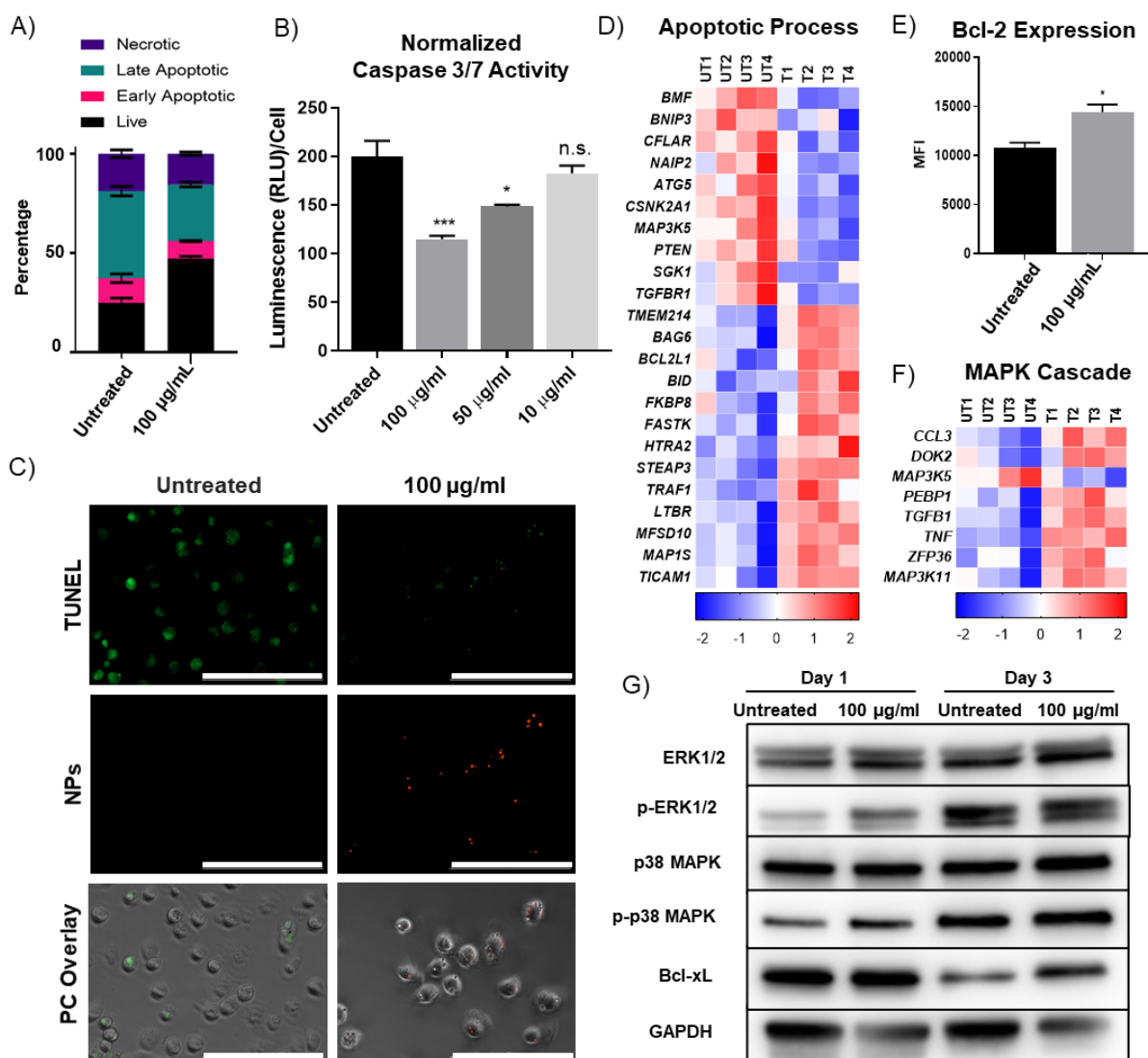
792

793 **Figure 1: Phagocytosis of inert PEGDA NPs promotes longevity of primary macrophages *ex***
 794 ***vivo*.** A) Microscopy images at 20x magnification of BMMs treated with NPs (green fluorescence)
 795 showing enhanced survival compared to untreated cells for over 115 days. Scale bar 100 µm. B)
 796 Metabolic Activity of BMMs one and two weeks after treatment with different concentrations of
 797 PEGDA NPs. CellTiter-Glo® 2.0 Cell Viability Assay was used to determine cell viability
 798 measured through luminescence. *p<0.05, **p<0.01, #p<0.0001 (compared to untreated cells)
 799 using Dunnett's multiple comparisons test as part of a two-way ANOVA. C) Cell counts of BMMs
 800 one and two weeks after treatment with different concentrations of PEGDA NPs. n.s. is not
 801 significant, *p<0.05, #p<0.0001 (compared to untreated cells) using Dunnett's multiple
 802 comparisons test as part of a two-way ANOVA (N=6). D) Cell counts of BMMs treated with 100
 803 µg/ml NPs of varying composition one week following NP treatment. *p<0.05, **p<0.01,
 804 ***p<0.001, ****p<0.0001 using Dunnett's multiple comparisons test as part of a one-way
 805 ANOVA. E) Cell counts of *ex vivo* alveolar macrophages three weeks after treatment with 100
 806 µg/ml PEGDA NPs. **p<0.01 using a student's T-test. F) Cell counts of *ex vivo* peritoneal
 807 macrophages three weeks after treatment with 100 µg/ml PEGDA NPs. *p<0.05 using a student's
 808 T-test. In all graphs, unless stated otherwise, bars represent the mean and error bars represent SEM
 809 (N=3); Data are representative of two independent experiments.

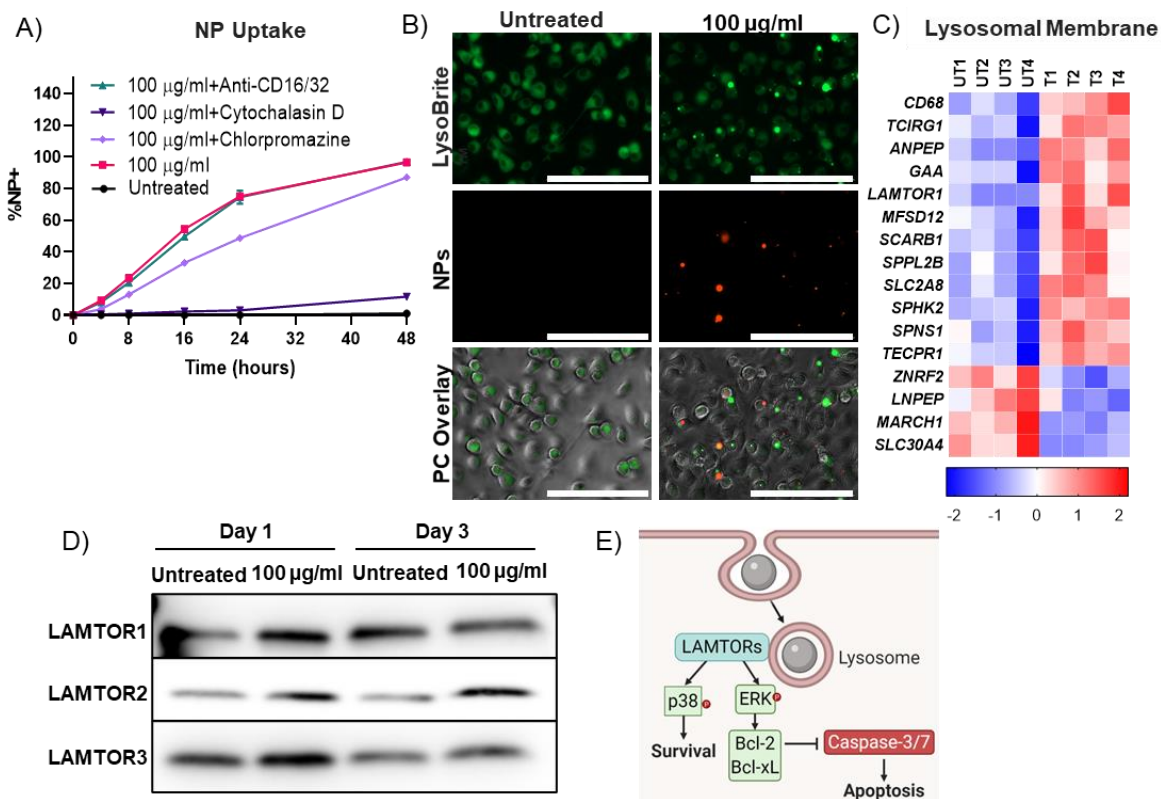
810



811
812 **Figure 2: Phagocytosis of PEGDA NPs promotes macrophage immune functionality.** A)
813 MHCII marker expression of M0, M1, and M2 BMMs 24 hours following treatment with 100
814 μ g/ml NPs (patterned bars). Data are representative of two independent experiments. B) Row Z-
815 scores of gene counts from RNAseq analysis in Immune System Process GO term of NP-treated
816 BMMs (T) compared to untreated BMMs (UT) showing four biological replicates per group. C)
817 IL-6 and TNF- α concentrations of BMM supernatants four week following NP treatment after LPS
818 challenge for 24 hours. In all plots, bars represent the mean and error bars represent SEM ($N=3$).
819 * $p<0.05$, ** $p<0.01$, *** $p<0.001$ using student's T-test.
820



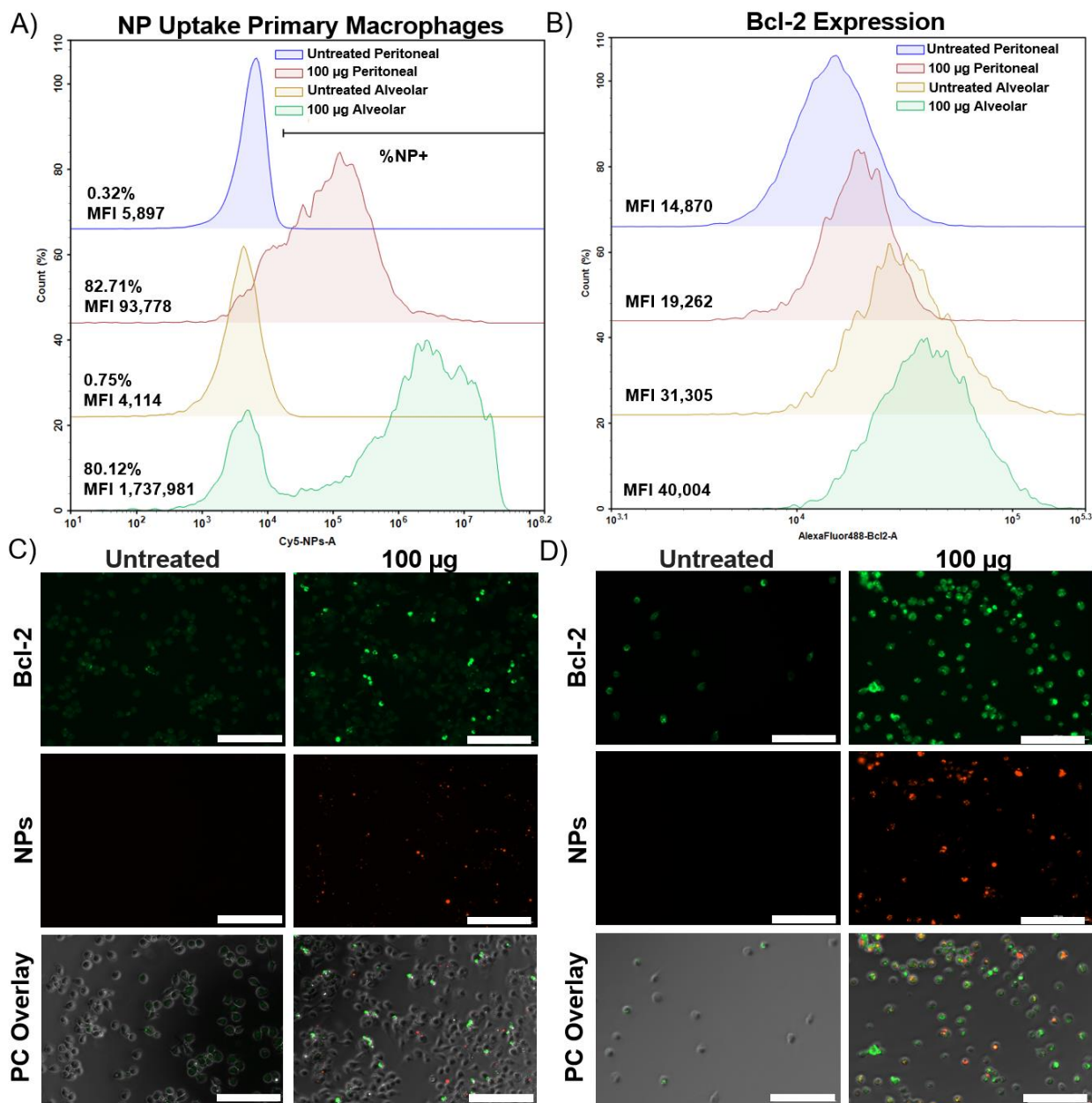
821
 822 **Figure 3: Treatment with PEGDA NPs suppresses apoptosis in primary macrophages.** A)
 823 Representative flow cytometric quadrant analysis of modes of cell death in BMMs 72 hours
 824 following NP treatment based on Annexin V and Zombie Yellow dual staining. B) Normalized
 825 caspase 3/7 activity measured using Caspase-Glo® 3/7 Assay System 72 hours following NP
 826 treatment of varying concentrations. n.s. is not significant, *p<0.05, ***p<0.001 (compared to
 827 untreated cells) using Dunnett’s multiple comparisons test as part of a one-way ANOVA. Bars
 828 represent the mean and error bars represent SEM (N=3). C) TUNEL apoptosis imaging analysis of
 829 untreated or NP-treated BMMs 24 hours following NP treatment at 40x magnification. Scale bar
 830 100 µm. Phase Contrast (PC). D) Row Z-scores of gene counts from RNAseq analysis in Apoptotic
 831 Process GO term of NP-treated BMMs (T) compared to untreated BMMs (UT) showing four
 832 biological replicates per group. E) Anti-apoptotic Bcl-2 protein expression 72 hours following NP
 833 treatment, measured by median fluorescent intensity (MFI) using Flow Cytometry. *p<0.05 using
 834 a student’s T-test. Bars represent the mean and error bars represent SEM (N=3). F) Row Z-scores
 835 of gene counts from RNAseq analysis in MAPK Cascade GO term of NP-treated BMMs (T)
 836 compared to untreated BMMs (UT) showing four biological replicates per group. G) Western blots
 837 of representative antiapoptotic proteins and members of MAPK cascades 1 day and 3 days
 838 following NP treatment. Data in A, B, E, and G are representative of two independent experiments.



839

840 **Figure 4: NP phagocytosis and lysosomal involvement in BMM survival.** A) Kinetic NP uptake
 841 analysis and effect of internalization inhibitors on cell uptake. Error bars represent SEM ($N=3$). B)
 842 Row Z-scores of gene counts from RNAseq analysis in Lysosomal Membrane GO term of NP-
 843 treated BMMs compared to untreated BMMs showing four biological replicates per group. C)
 844 Lysosomal tracking and imaging at 40x magnification with LysoBrite™ Green 24 hours following
 845 NP treatment. Scale bar 100 μ m. Phase Contrast (PC). D) Western blotting of LAMTOR1, 2, and
 846 3 lysosomal proteins 1 day and 3 days following NP treatment. E) Schematic of hypothesized
 847 effect of NP phagocytosis on macrophage survival.

848



849
 850 **Figure 5: NP phagocytosis *in vivo* upregulates anti-apoptotic Bcl-2 protein in alveolar and**
 851 **peritoneal macrophages.** A) Cy5-labeled NP internalization in peritoneal macrophages and
 852 alveolar macrophages. %NP+ cells and MFI (median fluorescence intensity) are indicated. B)
 853 Flow cytometric analysis of Bcl-2 expression in *in vivo* NP-treated peritoneal macrophages and
 854 alveolar macrophages. Data are representative of two independent experiments. Fluorescent
 855 imaging at 20x magnification after immunostaining with anti-Bcl-2 antibodies 24 hours following
 856 dosing of 100 μ g of NPs to mice: C) Peritoneal macrophages D) Alveolar macrophages. Scale bar
 857 100 μ m. Phase Contrast (PC).